ACS OMEGA

http://pubs.acs.org/journal/acsodf

Article

Scalable Preparation of Sub-Millimeter Double-Shelled Al_2O_3 Hollow Spheres and Their Rapid Separation from Wastewater after Adsorption of Congo Red

Jiawei Yan,[#] Xinshuang Guo,[*,#] Haifeng Guo,[*] Li Wan, Tao Guo, Zhaolong Hu, Pengfei Xu, Huilong Chen, Shuning Zhu, and Qianglong Fei

Cite This: *ACS Omega* 2022, 7, 37629−37639

Read Online

ACCESS | Metrics & More | Article Recommendations | Supporting Information

ABSTRACT: Porous double-shelled ceramic hollow spheres (PDSs) have attracted extensive attention due to their high specific surface areas and multifunctional designs. When used in wastewater treatment, millimeter or sub-millimeter spheres can be quickly separated from water by commercial sieves. However, the simple, scalable, and low-cost preparation of sub-millimeter PDSs in the solid phase remains a challenge. Herein, porous PDSs were facilely fabricated via a spheronization process utilizing pseudoboehmite powders and wet gelatin spheres as templates, which broke through the difficulty of preparing PDSs by one-step solid-state synthesis. Treating pseudoboehmite powder with nitric acid can improve the compressive strength of the PDSs. By controlling the rolling time and gelatin concentration of gelatin microspheres, the integrity, shell thickness, and double-shelled spacing of the gelatin microspheres were tuned. When the rolling time was 8−12 min, and the gelatin concentration in gelatin spheres was 250 g/L, and PDSs with a complete double-shelled structure, good mechanical property, and high specific surface area (327.5−509.6 m^2/g) were obtained at 600 °C. The adsorption capacities of the PDSs for 100 mg/L Congo red solution (70.7 mg/g) were larger than those of single-shelled hollow spheres (49 mg/g), and larger diameters (608−862 μm) of the PDSs allow them to be rapidly separated from solution by a commercial sieve. This paper provides a facile and scalable method for the preparation of sub-millimeter PDSs and demonstrates their excellent adsorption capacity for Congo red solution.

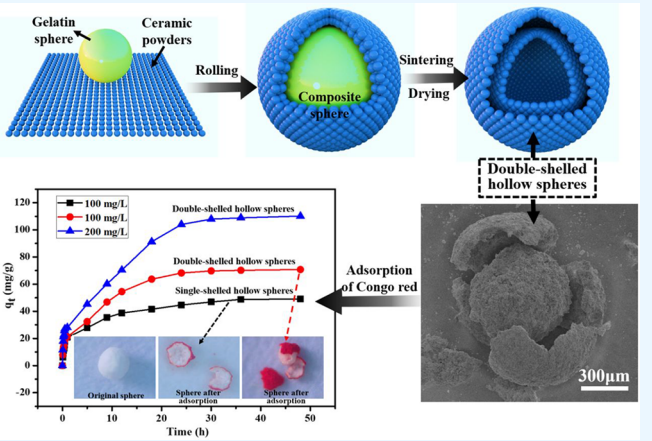

1. INTRODUCTION

Hollow spheres have attracted considerable interest due to their attractive properties such as a low density, high specific surface area, and high loading capacity,[1,2] which endows them with potential applications in supercapacitors,[3] catalysis,[4] sensors,[5] batteries,[6] and environmental remediation.[7] Three typical synthesis methods of hollow spheres include hard-templating methods,[8,9] soft-templating methods,[10] and template-free methods.[2] The hard-templating methods usually utilize "rigid" materials such as carbon spheres,[11] SiO_2 spheres,[12] gelatin spheres,[13] and so on as templates to prepare Co_3O_4@CdS,[14] Co_3O_4[11] $Ce_{1-x}Zr_xO_2$,[15] and RuO_2[16] hollow spheres. The soft template methods typically involve the formation of relatively flexible structures, such as emulsion droplets,[17] supramolecular micelles,[18,19] and vesicles[20] as templates. Huo et al. obtained hollow silica mesoporous spheres with an average diameter around 310 nm using cetyltrimethylammonium bromide vesicles as the template.[21] The template-free methods mainly use materials with self-assembly ability and annealing conditions to prepare hollow spheres.[22,23] Bao et al. prepared hollow TiO_2 spheres through a template-free solvothermal route using tetrabutyl titanate as the raw material and ethanol as the solvent.[24]

According to the sizes of the hollow spheres, they can be divided into nano-, micro-, and millimeter-scale hollow spheres.[25,26] In addition, according to the shell number of a single sphere, they can also be divided into single-shelled and multishelled hollow spheres.[1,27,28] Compared with the single-shelled hollow spheres, the multishelled ones have higher specific surface areas and multifunctional designs.[26,29] Yang et al. produced SnO_2/carbon composite spheres by chemically induced self-assembly in a hydrothermal environment and

Received: July 16, 2022
Accepted: October 4, 2022
Published: October 14, 2022

obtained multilayered SnO_2 hollow microspheres after sintering them.[30] Yuan et al. prepared TiO_2/SnO_2 double-shelled hollow spheres for efficient degradation of rhodamine B by a two-step liquid-phase deposition method using carbon sphere templates.[31] Zhang et al. obtained the hierarchical double-shelled NiO/ZnO hollow spheres by calcination of the metallic organic frameworks as a sacrificial template via a solvothermal method.[32] Although great efforts have been made to prepare multishelled hollow spheres, their preparation is mainly carried out in the liquid phase, gas phase, or a combination of liquid phase and solid phase,[1,26] and there are some problems such as high requirements for production equipment, complex processes, and so on.[33] Therefore, the simple and low-cost preparation of multishelled hollow spheres with industrial potential is still a bottleneck. Spheronization is a simple solid-phase method for preparing ceramic spheres or single-shell hollow spheres, similar to making snowballs by rolling solid powders, and has been industrialized.[34] However, a facile and scalable preparation of porous double-shelled ceramic hollow spheres (PDSs) by spheronization has not been investigated and remains a great challenge.

Toxic dyes such as Congo red (CR) in wastewater pose a serious threat to public health and ecological environments, and their removal is often performed by simple and low-cost adsorption methods.[32,35,36] γ-Al_2O_3 and one of its precursors, boehmite, have been used to treat dye wastewater due to their excellent adsorbability.[22] The diameters of double- or multi-shelled hollow spheres reported so far is 20 nm to 10 μm.[1,2,26] When these hollow spheres of small diameters are used as adsorbents to treat dye wastewater, it is difficult to separate them from water.[27] Sub-millimeter particles or spheres can be separated from the solution by a commercial sieve, but sub-millimeter double-shelled hollow spheres have not been reported yet.[34]

In this paper, for the first time, we utilized wet gelatin spheres with a high drying shrinkage as templates to uniformly attach pseudoboehmite powder to their surfaces, and then obtained the sub-millimeter Al_2O_3-based PDSs by spheronization and sintering. The effects of pseudoboehmite powders before and after nitric acid treatment on the structures and properties of solid ceramic spheres were studied. The effects of gelatin concentration in gelatin spheres and rolling time on the formation of the PDSs and their formation mechanism were investigated. The adsorption properties of the PDSs were evaluated by adsorption of CR from aqueous solution.

2. EXPERIMENTAL SECTION

2.1. Treatment of Pseudoboehmite Powders. Wet gelatin spheres were used as templates, and pseudoboehmite powders (denoted as P_0, D_{50} = 8.7 μm) were used as raw materials. Pseudoboehmite powders were treated with nitric acid to improve mechanical properties of the PDSs prepared with them. First, 5 g of P_0 was added to 45 mL of deionized water and stirred at 60 °C for 1 h, and then some nitric acid was added dropwise and stirred for 30 min. Next, the mixed solution after stirring stood for 24 h and then was dried at 110 °C for 12 h. Finally, the dried ceramic powders were ground for the preparation of ceramic spheres. The pseudoboehmite powders treated with 0.1, 0.2, and 0.3 mol/L nitric acid were labeled as P_1, P_2, and P_3, respectively.

2.2. Preparation of Wet Gelatin Spheres. First, gelatin was dissolved in deionized water at 50 °C to prepare gelatin solution, and 0.09 g/mL glucose monohydrate was added into it. Then, the mixture was dripped into soybean oil at 50 °C by a peristaltic pump at 10 rpm/min and stirred at 150 rpm/min for 30 min. The volume ratio of water to soybean oil was 1:5. Next, the upper oil phase was poured out after the stirred solution was cooled at 4 °C for 2 h, and the remaining gelatin spheres were washed in detergent. Finally, the washed gelatin spheres were cured in 38% formaldehyde solution for 10 min and then refrigerated for later use.

2.3. Preparation of the PDSs via Wet Gelatin Spheres As Templates. Pseudoboehmite powders were uniformly adhered to the surface of the monodisperse wet gelatin spheres, and then the excess powders were removed by sieving. The gelatin spheres coated with ceramic powders were put into a pelletizing machine (YB-400, Guangzhou Yangying, China) and rolled at a speed of 20 rpm/min to obtain composite spheres. The composite spheres finally were dried and sintered to obtain Al_2O_3-based PDSs

2.4. Characterization. The microstructures of ceramic spheres were observed by a scanning electron microscope (SEM, S8010, Hitachi). The crystalline phases of the samples were characterized via X-ray diffraction (XRD, D8 Advance, Bruker). The compressive strength of ceramic spheres was obtained using a universal testing machine (AGS-X-10 kN, Shimadzu). The compressive strength of the spheres is defined as the fracture load per their maximum cross-sectional area, and the average strength was obtained by measuring 10 samples for each at each data point,[37] which has been added in the revised manuscript. Fourier transform infrared (FTIR) spectroscopy was performed on a Nicolet iN10 FT-IR microscope (Thermo Nicolet Corp.). The morphologies and EDX analysis of the specimens were obtained on a transmission electron microscopy (TEM, JEOL-2100Plus). N_2 adsorption/desorption isotherms of samples were determined via a surface area analyzer (TriStar I13020, Micromerities). Pore size distribution and the specific surface area were obtained by the BJH method and BET method, respectively.

2.5. Adsorption Experiments. For adsorption tests, 30 mg of the treated hollow spheres was added into 100 mL of CR solution after they were treated in HCl solution at pH 4 for 2 h. The static adsorption of CR was carried out at different initial concentrations of CR solution at pH 4 and 25 °C. At appropriate time intervals, the analytical mixture was collected and separated. The remaining CR concentration in the aqueous phase was determined using an UV−visible spectrophotometer (Lambda 650S, PerkinElmer) around a wavelength of 500 nm. Adsorption capacity of CR on the spheres at time t (q_t) and at equilibrium (q_e) was calculated using the following eqs 1 and 2, respectively.

$$q_t = \frac{(C_0 - C_t)V}{M} \quad (1)$$

$$q_e = \frac{(C_0 - C_e)V}{M} \quad (2)$$

where C_0, C_t, and C_e (mg/L) are the concentrations of CR initially, at time t and at equilibrium, respectively. V (L) is volume of solution, and M (g) is mass of hollow spheres.

3. RESULTS AND DISCUSSION

3.1. Preparation and Optimization of the PDSs. *3.1.1. Structure and Performance Control of Solid Ceramic Spheres.* In order to study the effect of nitric acid treatment of pseudoboehmite powders on mechanical properties of ceramic

https://doi.org/10.1021/acsomega.2c04490
ACS Omega 2022, 7, 37629−37639

spheres, solid spheres were used instead of the PDSs as the research object to eliminate experimental errors caused by small diameters and thin shell of the PDSs.[17] The compressive strength of solid ceramic spheres obtained by rolling ceramic powders for 8 min and sintering is shown in Figure 1. When

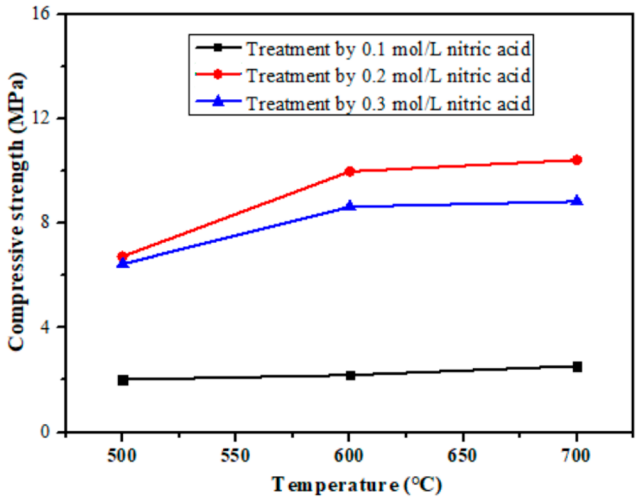

Figure 1. Compressive strength of solid ceramic spheres.

the sintering temperature is 600 °C, the compressive strength of the ceramic sphere prepared using P_0 is only about 0.25 MPa. However, when P_0 is treated with 0.1, 0.2, and 0.3 mol/L of nitric acid, the compressive strength of ceramic spheres prepared using the treated powders P_1, P_2, and P_3 is 2.19, 9.98, and 8.63 MPa, respectively. When pseudoboehmite is treated with nitric acid, FTIR spectra analysis shows that the functional groups on its surface do not change except for the peak intensity of NO_3^- (Figure S1), but its peptization is significantly improved (Figure S2). Peptization can improve the adhesion of ceramic particles after water absorption in wet gelatin, thereby increasing the compressive strength of ceramic spheres prepared with the treated powder. It is reported that the pore volume and specific surface area of pseudoboehmite treated with nitric acid increase little.[38] Therefore, the peptization increase of pseudoboehmite will improve the sphere strength far more than the decrease of its strength caused by the increase in pore volume of pseudoboehmite. As a result, the compressive strength of ceramic spheres prepared by pseudoboehmite treated with nitric acid is higher.[39] At the same temperature, the compressive strength of ceramic spheres prepared with P_2 is the highest. When it increases from 600 to 700 °C, the compressive strength of ceramic spheres increases slightly. Because the grain sizes increase slightly with the increase of temperature due to the aggregation of pseudoboehmite (Figure 3), the consequent increase in the bonding force between particles results in a slight increase in the compressive strength of ceramic spheres.[40]

Figure 2 shows the microstructures of ceramic spheres prepared from powders treated with different concentrations of nitric acid and sintered at 600 °C. In Figure 2a, the connections between the particles in ceramic spheres prepared using the untreated P_0 are relatively loose, and there are many pores on the surface of the particles. In Figure 2b,c, as the nitric acid concentration increases from 0.1 to 0.2 mol/L, the ceramic particles are closely connected, and the surface pore numbers of the particles increase, which results from the

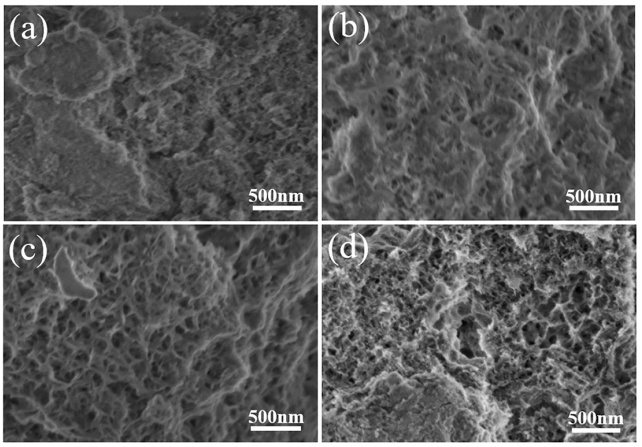

Figure 2. Microstructures of ceramic spheres prepared using powders treated with different concentrations of nitric acid: (a) 0 mol/L, (b) 0.1 mol/L, (c) 0.2 mol/L, and (d) 0.3 mol/L.

rearrangement of pore structures between the particles.[41] However, when the acid concentration used in the powder treatment is 0.3 mol/L, the uniformity of its pore structures becomes worse (Figure 2d). Because H^+ generated by the ionization of nitric acid solution reacts with the hydroxyl group of pseudoboehmite to form positively charged colloid. The colloid will attract other pseudoboehmite and form a network connection, which will reduce the fluidity of particles and turn them into sol.[42] The network connection between pseudoboehmite treated with 0.1 mol/L nitric acid is relatively less, resulting in small pore sizes and poor pore uniformity. However, after being treated with 0.3 mol/L nitric acid, they will undergo sufficient gelation reaction, the original accumulation of pseudoboehmite will be destroyed, and the micropores will increase and combine into nonuniform macropores.[39] Therefore, when pseudoboehmite powders are treated with nitric acid of 0.2 mol/L, the ceramic spheres prepared with the treated powders P_2 have relatively good pore uniformity and compressive strength.

In order to identify phase structures of pseudoboehmite before and after nitric acid treatment and during sintering, Figure 3 shows XRD patterns of pseudoboehmite powders

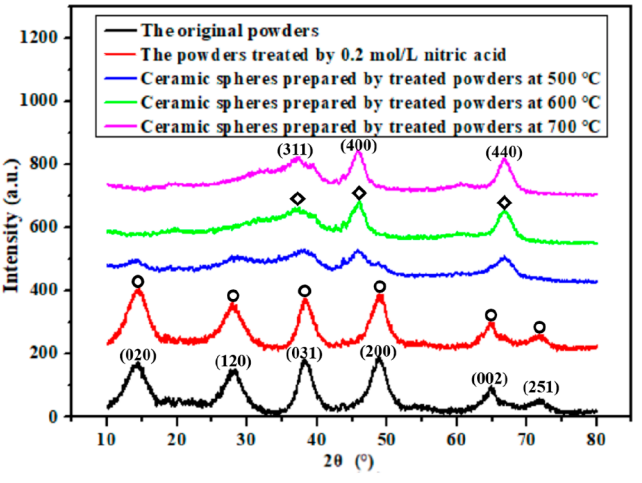

Figure 3. XRD patterns of pseudoboehmite powders before and after treatment with 0.2 mol/L nitric acid and ceramic spheres prepared with the treated powders.

https://doi.org/10.1021/acsomega.2c04490
ACS Omega 2022, 7, 37629−37639

before and after treatment with 0.2 mol/L nitric acid and ceramic spheres prepared using them at different temperatures. Pseudoboemite and γ-Al_2O_3 are marked with circles and diamonds, respectively. The characteristic peaks of pseudoboehmite powders before and after nitric acid treatment have no obvious change. When the sintering temperature is 500 °C, the crystal phase of ceramic spheres is mainly composed of pseudoboehmite and γ-Al_2O_3. When the temperature increases from 600 to 700 °C, the average grain size of pseudoboehmite obtained by Scherrer's formula increases from 3.78 to 4.28 nm.[43] As the temperature increases, its pore volume decreases with the loss of part of the oxygen sublattice, and the grain growth rate increases, resulting in the increase in grain size.[44] In addition, the crystal phase of the prepared ceramic sphere is γ-Al_2O_3, which is consistent with the reported results.[45] Since high temperature can reduce the porosity of ceramics[9] and ceramic spheres have a high strength at 600 °C, the PDSs below were prepared at 600 °C.

3.1.2. Structure Regulation of the PDSs. As the gelatin concentration increases, the diameters of gelatin spheres gradually increase (Figure S3), and their volume shrinkage decreases after drying (Figure S4), which is beneficial to regulate the structures of the PDSs based on them. Figure 4

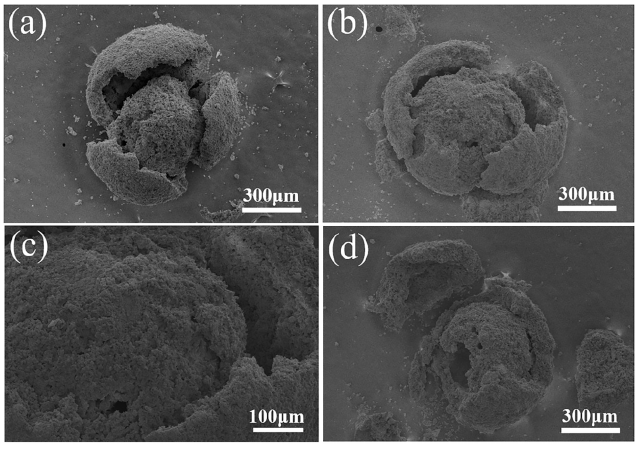

Figure 4. Morphologies of the PDSs prepared using gelatin spheres with different gelatin concentrations as templates: (a) 150 g/L, (b, c) 250 g/L, and (d) 350 g/L.

shows the interior of the cleaved PDSs prepared using gelatin spheres with different gelatin concentrations as templates, and the morphologies of the intact PDSs are shown in Figure S5. It should be noted that due to the large diameters (>600 μm) and thick shell (>50 μm) of the PDSs, they do not meet TEM imaging requirements, so SEM imaging is used instead of TEM imaging to characterize the double-shelled structures of the PDSs. In addition, we split the intact PDSs to study their double-shell structures. When the gelatin concentration in gelatin spheres is 150 g/L, the double-shelled spacing of the prepared PDSs is 60−105 μm (Figure 4a), but some of double-shelled structures are incomplete. This is mainly due to the excessive drying shrinkage of gelatin spheres with a lower gelatin concentration,[46] resulting in an incomplete inner shell of the PDS and easy damage. In Figure 4b,c, the PDSs prepared using gelatin spheres with a gelatin concentration of 250 g/L as templates are relatively intact and show an obvious double-shelled structure. The PDS can also be prepared using gelatin spheres with a gelatin concentration of 350 g/L (Figure 4d), but its double-shelled spacing is only 10−50 μm, and sometimes only single-shelled hollow spheres can be prepared. Therefore, the use of gelatin spheres with a gelatin concentration of 250 g/L is beneficial to obtain PDSs with the complete structure and suitable double-shelled spacing. The morphologies of more PDSs prepared using gelatin spheres with different gelatin concentration as templates are shown in Figures S6−S8.

The morphologies and structural parameters of the PDSs prepared at different rolling times using gelatin spheres with a gelatin concentration of 250 g/L as templates are shown in Figure 5 and Table 1, respectively. The spheroidization process

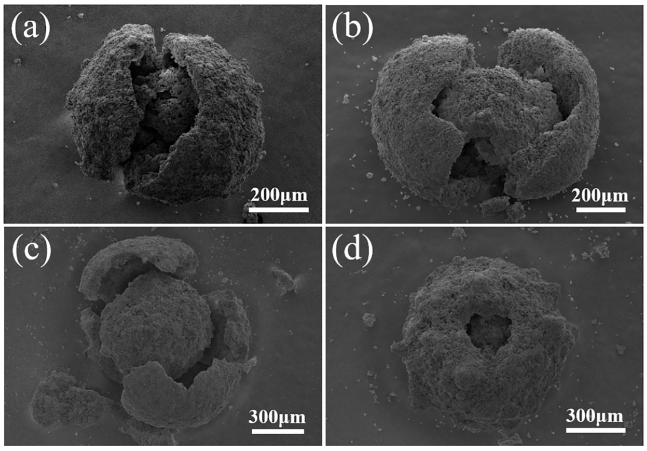

Figure 5. Morphologies of the PDSs prepared using gelatin spheres with a gelatin concentration of 250 g/L as templates at different rolling times: (a) 4 min, (b) 8 min, (c) 12 min, and (d) 16 min.

Table 1. Structural Parameters of the PDSs Prepared Using Gelatin Spheres with a Gelatin Concentration of 250 g/L as Templates at Different Rolling Times

structural characteristics of PDSs	PDSs prepared with a rolling time of 4 min	PDSs prepared with a rolling time of 8 min	PDSs prepared with a rolling time of 12 min	PDSs prepared with a rolling time of 16 min
integrity	no	yes	yes	no
amount	a little	much	much	little
diameter	604−776 μm	608−862 μm	689−807 μm	668−797 μm
proportion of external shell	11−17%	15−23%	12−21%	7−11%
proportion of double-shelled spacing	12−21%	14−22%	8−17%	5−9%

can influence structures of the final spheres.[34] When the rolling time is 4 min, the amount of the prepared PDSs is small, and their integrity is poor (Figure 5a). When the rolling time is 8 min, the sphericity and double-shelled structure of the PDSs are better (Figure 5b), and the total thickness of their outer shells account for 15−23% of its diameter. With the increase of rolling time, the arrangement of ceramic particles adhered to the surfaces of gelatin spheres becomes compact due to the interparticle bond,[47] and it is beneficial to the formation of the PDSs. When the rolling time is 12 min, the double-shelled structures of the prepared PDSs are still relatively complete (Figure 5c). However, when the rolling time is 16 min, the surfaces of the outer shells of the PDSs are nonuniform, and their total thickness is only 7−11% of the diameters (Figure

https://doi.org/10.1021/acsomega.2c04490
ACS Omega 2022, 7, 37629−37639

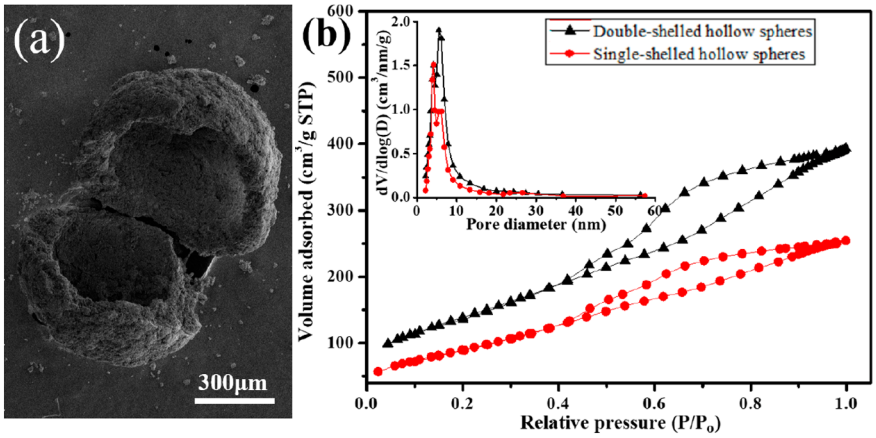

Figure 6. (a) Morphology of the SHS; (b) N_2 adsorption/desorption isotherms and pore size distribution (inset) of the DHSs and the SHSs.

5d), which is due to the falling of ceramic powders adherring to the surfaces of gelatin spheres when the rolling time is too long. It is seen that the suitable rolling time for preparing the PDSs is 8−12 min. Therefore, with the increase of rolling time, the integrity and shell thickness of the PDSs first increase and then decrease, and their double-shelled spacing gradually decreases.

3.1.3. N_2 Adsorption/Desorption and TEM Characterization of the PDSs. The specific surface areas and pore size distribution of single- and double-shelled hollow spheres are studied below. The preparation of double-shelled hollow spheres follows main parameters, such as P_2 powders, gelatin spheres with a gelatin concentration of 250 g/L, a rolling time of 8 min, and a sintering temperature of 600 °C, and the resulting double-shelled hollow spheres are labeled as DHSs. Similarly, the preparation process of single-shelled hollow spheres is the same as that of the DHSs except that 5 wt % of sodium polyacrylate is added to the P_2 powders, and the resulting single-shelled hollow spheres are marked as SHSs, and a SHS is exhibited in Figure 6a. The influence of adding sodium polyacrylate to ceramic powders on structures of the PDSs is shown in Figure S9.

The N_2 adsorption/desorption isotherms and pore size distribution of the SHSs and the DHSs are presented in Figure 6b. Their isotherms can be classified as type IV, suggesting the shell of the hollow spheres with mesopores.[48,49] According to the pore size distribution curve of the two samples (inset in Figure 6b), it is shown that they have uniform pore size distribution mainly in the range of 2.5−10 nm, which is consistent with the results in Figure 3. The BET surface area of the double-shelled hollow sphere (509 m^2/g) is larger than those of the single-shelled hollow spheres (333 m^2/g), indicating that the presence of two shells in the former contributes to the increase of BET surface areas.[50]

TEM image of the DHS shows the apparent nanopores in its shell in Figure 7a, which is in accordance with results of pore size distribution in Figure 6b. The element composition of the DHS is further identified by EDX spectrum (Figure 7b), suggesting the presence of Al and O elements. As shown in EDX element mappings in Figure 7c,d, Al and O elements are evenly dispersed on the DHS. Obviously, the pseudoboehmite forming spheres is transformed into Al_2O_3 after the calcination and pyrolysis of gelatin spheres,[51] which further confirms the successful synthesis of γ-Al_2O_3 spheres.

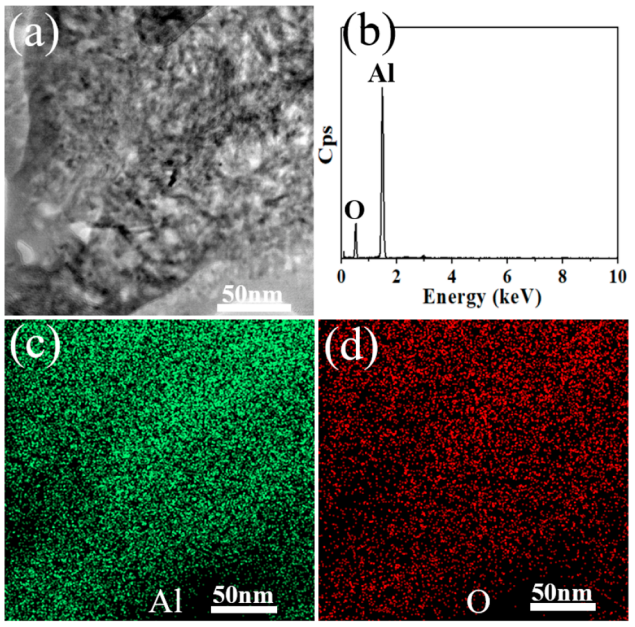

Figure 7. (a) TEM image; (b) EDX spectrum; and (c, d) element mapping of the DHS.

3.2. Formation Mechanism of the PDSs. Figure 8 shows the formation mechanism of the PDS. When the wet gelatin sphere is put into ceramic powders (Figure 8a), the powders will adhere to its surface and form a loose powder layer on it. Due to the mutual extrusion between ceramic particles in the spheronization process,[47] the arrangement of the particles in this layer becomes compact on the outside and relatively loose on the inside (Figure 8b), and the inner loose layer is separated from the outer tight layer with the shrinkage of wet gelatin spheres during drying. When the gelatin sphere is completely dried, a composite sphere consisting of a hollow sphere formed by ceramic powders, and a gelatin sphere adhered with ceramic powders inside is obtained (Figure 8c and Figure S10). After sintering the composite spheres to exclude gelatin spheres, the PDS is obtained (Figure 8d). To sum up, the specific surface area, bulk density, and porosity of the as-prepared PDSs are 327.57−509.64 m^2/g, 0.69−0.84 g/cm^3 and 76−85%, respectively.

3.3. Adsorption Properties of the PDSs. Figure 9 shows the time dependency of the adsorption of CR on the DHSs

https://doi.org/10.1021/acsomega.2c04490
ACS Omega 2022, 7, 37629−37639

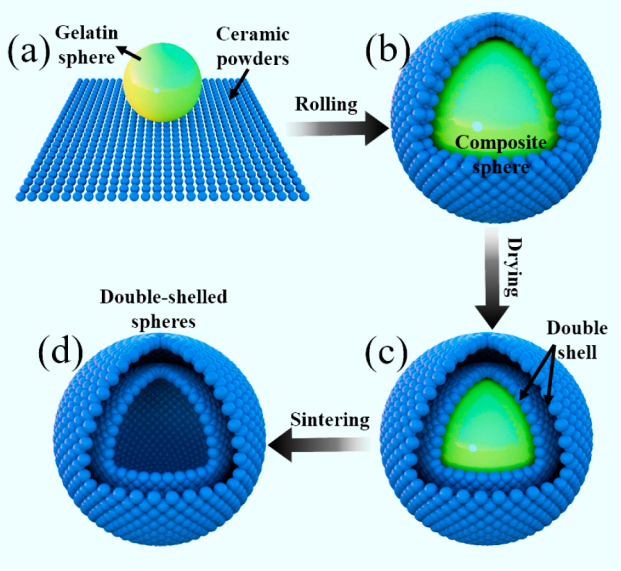

Figure 8. Formation mechanism of the PDS: (a) putting the gelatin sphere into ceramic powders, (b) composite sphere consisting of gelatin sphere and ceramic powder layer adhered to its surface prepared by rolling, (c) separation of the inner and the outer of ceramic powder layer after drying, (d) the PDS obtained after sintering.

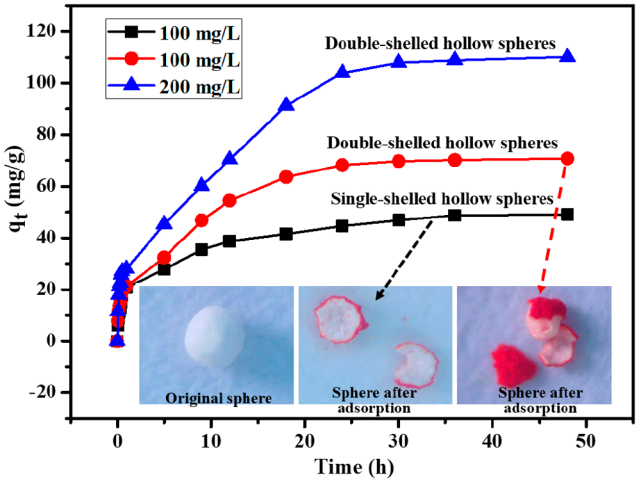

Figure 9. Static adsorption capacity of the DHSs and the SHSs for CR removal with the changes of the initial concentration and contact time at 25 °C; the inset shows pictures of the original sphere and the spheres after adsorption at a CR concentration of 100 mg/L for 48 h.

and the SHSs at different initial concentrations (100 and 200 mg/L). During the initial 0.5 h, the adsorption capacity of the three samples increases dramatically, indicating more adsorption sites in them for accommodating the CR anions.[52] When the contact time is further increased to 24 h, their adsorption capacity increases steadily and tends to be stable in the subsequent time, indicating the existence of adsorption equilibrium and the gradual depletion of adsorption sites.[53,54] When CR concentration is 100 mg/L, the DHSs have a larger adsorption capacity (70.7 mg/g) compared with the SHSs (49 mg/g). The inset of Figure 9 shows the morphologies of the DHSs and the SHSs before and after the adsorption of 100 mg/L of CR. The initial hollow spheres are white, but after adsorption of CR, the outer surface of their shell is dark red, and the inner gradually changes to a light color. Compared with SHSs, DHSs are not only light red in the inner color of the outer shell, but also the outer color of the inner shell is light red. It is clear that the inner shell is also involved in the adsorption of CR. In addition, the adsorption capacity of the DHSs increases to 110.1 mg/g with the increase of the CR concentration from 100 to 200 mg/L, which means that the double-shelled hollow spheres are efficient at removing CR in aqueous solution.

3.4. Kinetics, Isotherms, and Mechanism of Adsorption. In order to study the control mechanism of the CR adsorption process, the pseudo-first-order, pseudo-second-order, and Elovich kinetic models are utilized to investigate the adsorption kinetics of CR on PDSs. The equations of the three kinetic models refer to refs 55 and 56, and their fitting curves and parameters are shown in Figure 10a and Table 2. Because their correlation coefficients (R^2) are higher than 0.90, the adsorption of CR on three samples accords with the second-order kinetic and Elovich models, which indicates that their adsorption of CR is controlled by a variety of adsorption mechanisms.[57] In addition, the adsorption capacity (q_e, cal) obtained by the pseudo-second-order kinetic model is very close to the experimental value (q_e, exp), which means that the chemisorption reaction or activation process dominates the CR adsorption process.[58]

Kinetic plots of Weber−Morris particle diffusion model for the adsorption of CR with different initial concentrations on the PDSs are shown in Figure 10b, and the equation of this model is referred to ref 57. The three linear segments indicate that the adsorptive mass transfer proceeds by rapid external surface adsorption (K_{d1} region), gradual pore diffusion or intraparticle diffusion (K_{d2} region), and the slow or equilibrium adsorption on the interior surface of the PDSs (K_{d3} region).[59] The segment slope is defined to the intraparticle diffusion rate constants (K_d). $K_{d1} > K_{d2} > K_{d3}$ in Figure 10b indicates that the adsorption of CR is more dependent on the boundary layer thickness.[60]

The isotherm data are analyzed by the Langmuir equations (eq 3), Freundlich equations (eq 4), Temkin and Dubinin−Radushkevich (D-R) equation, and the Temkin and D-R isotherm equation can be found in refs 50, 51, and 61.

$$q_e = \frac{q_m . K_L . C_e}{1 + K_L . C_e} \quad (3)$$

$$q_e = K_F . C^{1/n} \quad (4)$$

where q_e (mg/g) and q_m (mg/g) refer to the equilibrium adsorption capacity and theoretical maximum adsorption capacity, respectively. K_L and K_F refer to the constants of Langmuir and Freundlich equations, respectively, and n is the adsorption intensity. Figure 11a shows the plots of four isotherms for CR adsorption on the DHSs and the fitted parameters of each isotherm. It is noticeable that th eLangmuir isotherm is more suitable for CR adsorption on the spheres because of its higher correlation coefficient (R_2, 0.995), which implies the monolayer coverage of CR on the spheres.[52,62] The uptake equilibrium is calculated by the Langmuir equation with a maximum adsorption capacity of CR (133.1 mg/g). The n value obtained from the Freundlich isotherm is greater than 2, indicating that the DHSs have good adsorption and can act as a good adsorbent for CR adsorption.[63]

https://doi.org/10.1021/acsomega.2c04490
ACS Omega 2022, 7, 37629−37639

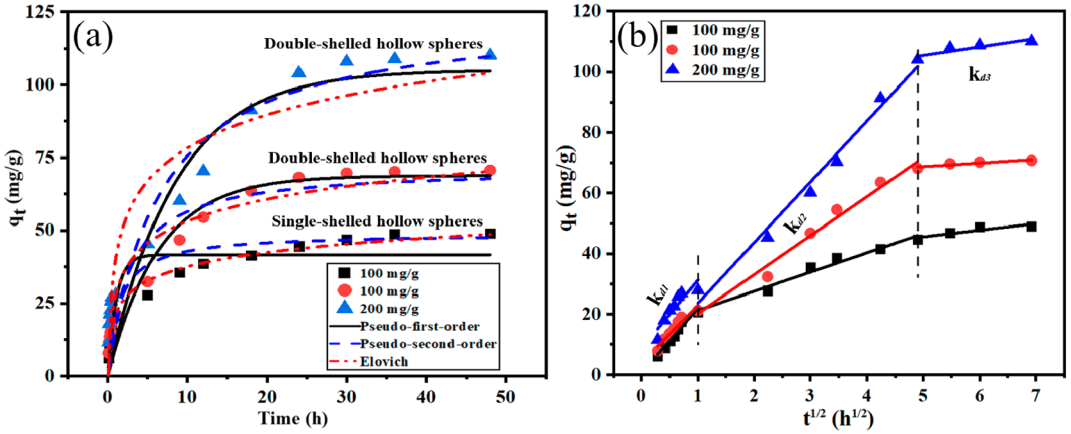

Figure 10. Kinetic plots of (a) the pseudo-first-order, pseudo-second-order, and Elovich kinetic models, (b) Weber−Morris particle diffusion model for the adsorption of CR on the PDSs.

Table 2. Adsorption Kinetic Parameters of the Kinetic Models Utilized for the Adsorption of CR on the PDSs

			pseudo-first-order model			pseudo-second-order model			Elovich model		
adsorbent	C_0(mg/L)	$q_{e.\ exp}$(mg/g)	$q_{e.\ cal}$(mg/g)	k_1	R^2	$q_{e.\ cal}$(mg/g)	k_2	R^2	α	β	R^2
SHSs	100	49.06	41.63	0.946	0.881	49.02	0.014	0.917	144.26	0.142	0.988
DHSs	100	70.71	68.82	0.156	0.890	71.57	0.005	0.925	140.34	0.091	0.957
DHSs	200	110.13	105.09	0.119	0.881	124.49	0.001	0.900	193.67	0.061	0.921

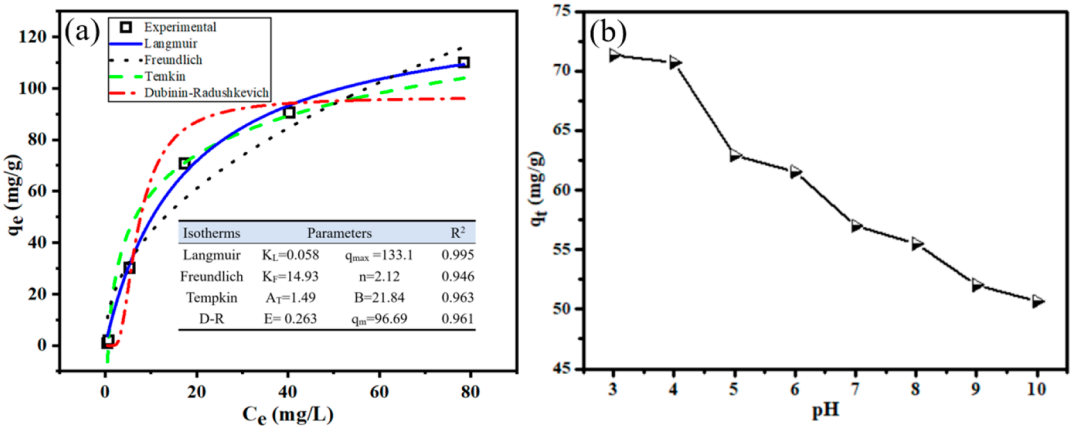

Figure 11. (a) Adsorption isotherms and parameters for the adsorption of CR on the DHSs; (b) effect of pH on adsorption of CR on the DHSs.

FTIR spectra of the CR and the PDSs before and after adsorption of CR are shown in Figure 12. The peaks of the initial PDSs at 3468 and 1637 cm^{-1} are attributed to the stretching vibration of theirs surface hydroxyl group (Figure 12b), and the peak intensity decreases after adsorption of CR, indicating that the hydroxyl groups are involved in the adsorption process.[64] The stretching vibrations of N−H and −N═N− assigned to 3463 and 1595 cm^{-1} peaks of CR are also weakened, indicating that hydrogen bonds are formed between hydroxyl groups of the PDS and -NH_2 or −N═N− groups of CR.[64,65] The new peak at 1045 cm^{-1} in Figure 12c belongs to the −S═O groups of CR, which confirms that the sulfonic group is also involved in CR adsorption.[65]Figure 11b shows the effect of pH of the CR solution (100 mg/L) on the equilibrium adsorption capacities of DHSs. The adsorption capacities of DHSs decrease slightly with the increase of the pH value from 3 to 4, while they decrease significantly as the pH value ranges from 5 to 10. Since the zero-charge point of Al_2O_3 is reported to be close to 9,[66] the electrostatic attraction between the positively charged surface of DHSs and anionic dye ions decreases with the pH increase. Therefore, the electrostatic attraction between PDSs and CR, and hydrogen bonds between hydroxyl groups of the PDSs and the amino groups, sulfonic groups, and −N═N− of CR mainly affect the adsorption of CR on the PDSs.

Table 3 shows the adsorption capacity and diameters of the as-prepared DHSs and some previously reported adsorbents used for CR and methylene blue (MB) removal from aqueous solutions. Compared with the reported submicron adsorbents, although the diameters (608−862 μm) of the DHSs are close to the millimeter scale, they have competitive or even excellent static adsorption performance without stirring and heating, and they can even be rapidly separated from the treatment solution (Figure 13 and inset of Figure 9) through a 60-mesh sieve due to their larger diameters.[67] In addition, a comparable recycling adsorption capacity for the regenerated DHSs is shown in Figure S11. Therefore, the double-shelled hollow spheres can serve as a promising candidate for wastewater treatment.

https://doi.org/10.1021/acsomega.2c04490
ACS Omega 2022, 7, 37629−37639

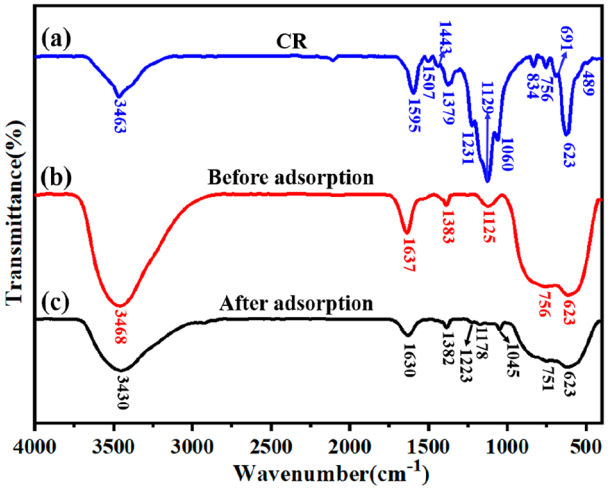

Figure 12. FTIR spectra of (a) the CR and the PDSs (b) before and (c) after adsorption of CR.

Table 3. Comparison of Adsorption Capacity and Diameters of the DHSs and Other Reported Adsorbents for CR and MB Removal

adsorbent	dyes	q_{max} (mg/g)	diameter (μm)	ref
DHSs sample	CR	133.1	608−862	this work
nanorod-like mesoporous γ-Al_2O_3	CR	83.8	0.01−0.02	68
hierarchical γ-AlOOH	CR	99	3−4	69
Co_3O_4−Fe_3O_4 hollow spheres	CR	123	1−2	70
porous ZrO_2 hollow spheres	CR	60	1−2	71
ZnO-modified SiO_2 nanospheres	CR	83	0.2−0.5	72
modified graphitic carbon spheres	MB	681.4	0.35	73
N-doped carbon sub-microspheres	MB	812.2	0.1−0.3	74

4. CONCLUSION

Sub-millimeter Al_2O_3-based PDSs were prepared by spheronization and sintering wet gelatin spheres adhered with pseudoboehmite powders. When the pseudoboehmite powders were treated with 0.2 mol/L nitric acid, the compressive strength of the solid ceramic spheres prepared with the treated powders at 600 °C was about 39.9 times higher than that of the solid spheres prepared with untreated powders. The double-shelled spacing of PDSs decreased with increasing gelatin concentration in gelatin spheres. Moreover, with the increase of rolling time, the integrity and shell thickness of the PDSs first increased and then decreased, and their double-shelled spacing gradually decreased. When the rolling time was 8−12 min, the amount of PDSs was large, and their structures were complete. Compared with single-shelled ceramic hollow spheres, the PDSs showed a larger adsorption capacity toward Congo red, resulting from their unique double-shelled structure and high specific surface area (327.5−509.6 m^2/g). The larger diameters (608−862 μm) of the PDSs enabled their rapid separation from the treatment solution by commercial sieves. This paper provides a facile and scalable method for fabrication of sub-millimeter PDSs and shows that they are a promising candidate for wastewater treatment.

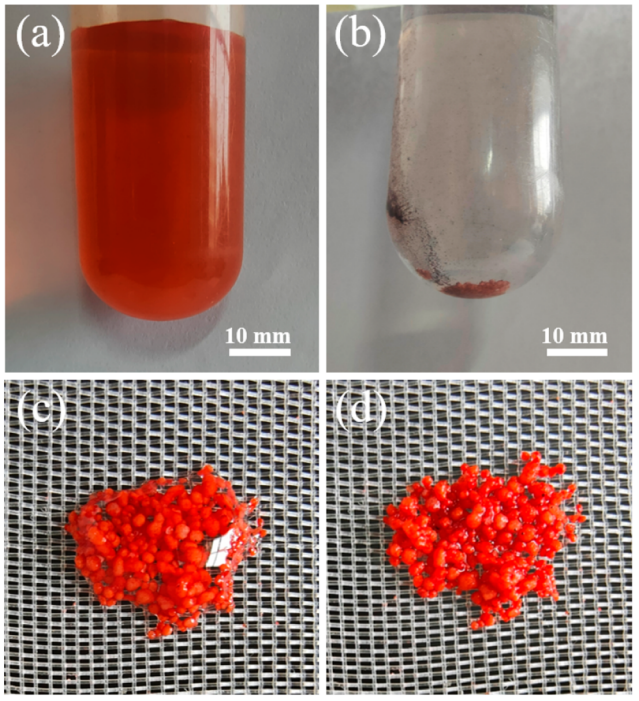

Figure 13. Photographs of the solution after centrifugation: (a) the initial CR solution, (b) solution after adsorption of CR by the DHSs; (c, d) separating the DHSs rapidly from solution by filtration through a 60-mesh sieve.

■ ASSOCIATED CONTENT

Supporting Information

The Supporting Information is available free of charge at https://pubs.acs.org/doi/10.1021/acsomega.2c04490.

FTIR spectra of pseudoboehmite before and after treatment; photograph of the treated pseudoboehmite powders; structures of gelatin microspheres and the PDSs; influence of adding a binder to ceramic powders on structures of the PDSs; formation of double-shelled structures of composite spheres during drying; recyclability (PDF)

■ AUTHOR INFORMATION

Corresponding Authors

Xinshuang Guo − *Jiangxi Key Laboratory of Industrial Ceramics, Engineering Technology Research Centre for Environmental Protection Materials and Equipment of Jiangxi Province, Pingxiang University, Pingxiang 337055, China*; orcid.org/0000-0001-6912-9417; Email: xsguo12b@alum.imr.ac.cn

Haifeng Guo − *Jiangxi Key Laboratory of Industrial Ceramics, Engineering Technology Research Centre for Environmental Protection Materials and Equipment of Jiangxi Province, Pingxiang University, Pingxiang 337055, China*; Phone: +86 07996682171; Email: guohaifeng720@163.com; Fax: +86 07996682171

Authors

Jiawei Yan − *Jiangxi Key Laboratory of Industrial Ceramics, Engineering Technology Research Centre for Environmental Protection Materials and Equipment of Jiangxi Province, Pingxiang University, Pingxiang 337055, China; Key Laboratory for Anisotropy and Texture of Materials*

https://doi.org/10.1021/acsomega.2c04490
ACS Omega 2022, 7, 37629−37639

(Ministry of Education), School of Materials Science and Engineering, Northeastern University, Shenyang 110819, China

Li Wan − *Jiangxi Key Laboratory of Industrial Ceramics, Engineering Technology Research Centre for Environmental Protection Materials and Equipment of Jiangxi Province, Pingxiang University, Pingxiang 337055, China; School of Mechatronics Engineering, Nanchang University, Nanchang 330031, China*

Tao Guo − *Jiangxi Key Laboratory of Industrial Ceramics, Engineering Technology Research Centre for Environmental Protection Materials and Equipment of Jiangxi Province, Pingxiang University, Pingxiang 337055, China*

Zhaolong Hu − *Jiangxi Key Laboratory of Industrial Ceramics, Engineering Technology Research Centre for Environmental Protection Materials and Equipment of Jiangxi Province, Pingxiang University, Pingxiang 337055, China*

Pengfei Xu − *Jiangxi Key Laboratory of Industrial Ceramics, Engineering Technology Research Centre for Environmental Protection Materials and Equipment of Jiangxi Province, Pingxiang University, Pingxiang 337055, China*

Huilong Chen − *Jiangxi Key Laboratory of Industrial Ceramics, Engineering Technology Research Centre for Environmental Protection Materials and Equipment of Jiangxi Province, Pingxiang University, Pingxiang 337055, China*

Shuning Zhu − *Jiangxi Key Laboratory of Industrial Ceramics, Engineering Technology Research Centre for Environmental Protection Materials and Equipment of Jiangxi Province, Pingxiang University, Pingxiang 337055, China*

Qianglong Fei − *Jiangxi Key Laboratory of Industrial Ceramics, Engineering Technology Research Centre for Environmental Protection Materials and Equipment of Jiangxi Province, Pingxiang University, Pingxiang 337055, China*

Complete contact information is available at: https://pubs.acs.org/10.1021/acsomega.2c04490

Author Contributions

[#]J.Y. and X.G. contributed equally.

Notes

The authors declare no competing financial interest.

■ ACKNOWLEDGMENTS

This work was supported by the National Natural Science Foundation of China (Nos. 21966026 and 52262009) and the Science and Technology Project of the Jiangxi Provincial Department of Education (No. GJJ202705), which are gratefully acknowledged.

■ REFERENCES

(1) Qi, J.; Lai, X.; Wang, J.; Tang, H.; Ren, H.; Yang, Y.; Jin, Q.; Zhang, L.; Yu, R.; Ma, G.; Su, Z.; Zhao, H.; Wang, D. Multi-shelled hollow micro-/nanostructures. *Chem. Soc. Rev.* **2015**, *44*, 6749−6773.

(2) Lai, X. Y.; Halpert, J. E.; Wang, D. Recent advances in micro-/nano-structured hollow spheres for energy applications: From simple to complex systems. *Energy Environ. Sci.* **2012**, *5*, 5604−5618.

(3) Lee, H.; Choi, J.; Myung, Y.; Lee, S. M.; Kim, H. J.; Ko, Y. J.; Yang, M. H.; Son, S. Yolk−shell polystyrene@ microporous organic network: a smart template with thermally disassemblable yolk to engineer hollow MoS_2/C composites for high-performance supercapacitors. *ACS omega* **2017**, *2*, 7658−7665.

(4) Liu, L.; Zhou, W.; Peng, Y.; Jiao, S.; Huang, Y.; Lv, J. Enhanced lubrication and photocatalytic degradation of liquid paraffin by hollow MoS_2 microspheres. *ACS Omega* **2018**, *3*, 3120−3128.

(5) Motsoeneng, R. G.; Kortidis, I.; Ray, S. S.; Motaung, D. E. Designing SnO_2 nanostructure-based sensors with tailored selectivity toward propanol and ethanol vapors. *ACS Omega* **2019**, *4*, 13696−13709.

(6) Gurunathan, P.; Ette, P. M.; Lakshminarasimhan, N.; Ramesha, K. A Convenient Synthesis Route for Co_3O_4 Hollow Microspheres and their application as a high performing anode in Li-ion batteries. *ACS Omega* **2017**, *2*, 7647−7657.

(7) Alsmaeil, A. W.; Hammami, M. A.; Enotiadis, A.; Kanj, M. Y.; Giannelis, E. P. Encapsulation of an anionic surfactant into hollow spherical nanosized capsules: size control, slow release, and potential use for enhanced oil recovery applications and environmental remediation. *ACS Omega* **2021**, *6*, 5689−5697.

(8) Li, C.; Ding, L.; Liang, C.; Zhang, J.; Zhang, C.; Mei, H.; Wang, C.; Wu, W.; Zhang, J.; Xu, W. Photon-induced light emission from foamed gold with micro/nanohollow sphere structures. *ACS Omega* **2017**, *2*, 5759−5765.

(9) Wan, L.; Guo, X. S.; Li, K.; Yan, J. W. Preparation of porous SiC-Al_2O_3 ceramics with spherical shell structures of large surface area and high strength. *Ceram. Int.* **2020**, *46*, 10325−10331.

(10) Rafati, A. A.; Borujeni, A. R. A.; Najafi, M.; Bagheri, A. Ultrasonic/surfactant assisted of CdS nano hollow sphere synthesis and characterization. *Mater. Charact.* **2011**, *62*, 94−98.

(11) Zhu, C.; Guan, S.; Li, W.; Ogunbiyi, A. T.; Chen, K.; Zhang, Q. Degradation of formaldehyde over MnO_2/CeO_2 hollow spheres: elucidating the influence of carbon sphere self-sacrificing templates. *ACS Omega* **2021**, *6*, 35404−35415.

(12) Wang, H. Q.; Gong, Q. H.; Huang, H.; Gao, T. T.; Yuan, Z. W.; Zhou, G. W. Pn heterostructured TiO_2/NiO double-shelled hollow spheres for the photocatalytic degradation of papermaking wastewater. *Mater. Res. Bull.* **2018**, *107*, 397−406.

(13) Ding, S. L.; ZHU, Y. H.; yang, X. L. Preparation of composite hollow microspheres on gelatin spheres as templates. *Journal of Inorganic Materials* **2004**, *19*, 991−996.

(14) Yang, H.; Fan, J.; Zhou, C.; Luo, R.; Liu, H.; Wan, Y.; Zhang, J.; Chen, J.; Wang, G.; Wang, R.; Jiang, C. Co_3O_4@ CdS hollow spheres derived from ZIF-67 with a high phenol and dye photodegradation activity. *ACS Omega* **2020**, *5*, 17160−17169.

(15) Jiang, H. X.; Huang, P.; Liu, L.; Zhang, M. H. Controllable synthesis of Ce1-xZr_xO_2 hollow nanospheres via supercritical anti-solvent precipitation. *Mater. Charact* **2012**, *63*, 98−104.

(16) Lee, W.-J.; Chun, Y.-G.; Jang, S.-J.; Paek, S. M.; Oh, J.-M. Hierarchical nanostructure of RuO_2 hollow spheres with enhanced lithium ion storage and cyclic performance. *J. Alloy. Compd.* **2017**, *711*, 611−616.

(17) Wang, H. Y.; Wang, F.; Liao, Q. L.; Li, X. B. Synthesis of millimeter-scale Al_2O_3 ceramic hollow spheres by an improved emulsion microencapsulation method. *Ceram. Int.* **2015**, *41*, 4959−4965.

(18) Goswami, M. M.; Dey, C.; Bandyopadhyay, A.; Sarkar, D.; Ahir, M. Micelles driven magnetite (Fe_3O_4) hollow spheres and a study on AC magnetic properties for hyperthermia application. *J. Magn. Magn. Mater.* **2016**, *417*, 376−381.

(19) Bao, Y.; Wang, T.; Kang, Q.; Shi, C.; Ma, J. Micelle-template synthesis of hollow silica spheres for improving water vapor permeability of waterborne polyurethane membrane. *Sci. Rep.* **2017**, *7*, 46638.

(20) Rajput, S. M.; Kuddushi, M.; Shah, A.; Ray, D.; Aswal, V. K.; Kailasa, S. K.; Malek, N. I. Functionalized surfactant based catanionic vesicles as the soft template for the synthesis of hollow silica nanospheres as new age drug carrier. *Surf. Interfaces* **2020**, *20*, 100596.

(21) Huo, W. L.; Zhang, X. Y.; Hu, Z. L.; Chen, Y. G.; Wang, Y. L.; Yang, J. L. Silica foams with ultra-large specific surface area structured by hollow mesoporous silica spheres. *J. Am. Ceram. Soc.* **2019**, *102*, 955−961.

(22) Wu, X. Y.; Zhang, B. Q.; Hu, Z. S.; Wang, F. Additive-free and time-saving microwave hydrothermal synthesis of hollow microspheres structured boehmite. *Adv. Powder Technol.* **2014**, *25*, 514−518.
(23) Luo, Y.; Zhang, X.; Huang, C.; Han, X.; Jiang, Q.; Zhou, T.; Yang, H.; Hu, J. $Zn_{0.8}Cd_{0.2}S$ Hollow spheres with a highly dispersed Ni dopant for boosting photocatalytic hydrogen generation. *ACS Omega* **2021**, *6*, 13544−13553.
(24) Bao, Y.; Kang, Q. L.; Ma, J. Z.; Liu, C. Monodisperse hollow TiO_2 spheres for thermal insulation materials: Template-free synthesis, characterization and properties. *Ceram. Int.* **2017**, *43*, 8596−8602.
(25) Qi, F.; Xu, X. X.; Xu, J.; Wang, Y. L.; Yang, J. L. A novel way to prepare hollow sphere ceramics. *J. Am. Ceram. Soc.* **2014**, *97*, 3341−3347.
(26) Hu, J.; Chen, M.; Fang, X.; Wu, L. Fabrication and application of inorganic hollow spheres. *Chem. Soc. Rev.* **2011**, *40*, 5472−91.
(27) Lou, X. W.; Archer, L. A.; Yang, Z. C. Hollow micro-/nanostructures: synthesis and applications. *Adv. Mater.* **2008**, *20*, 3987−4019.
(28) Huang, X.; Nan, Z. Synergetic adsorption and photo-Fenton degradation of methylene blue by $ZnFe_2O_4/SiO_2$ magnetic double-mesoporous-shelled hollow spheres. *Environ. Technol.* **2021**, *42*, 3218−3230.
(29) Wu, X. P.; Nan, Z. D. Degradation of rhodamine B by a novel Fe_3O_4/SiO_2 double-mesoporous-shelled hollow spheres through photo-Fenton process. *Mater. Chem. Phys.* **2019**, *227*, 302−312.
(30) Yang, H. X.; Qian, J. F.; Chen, Z. X.; Ai, X. P.; Cao, Y. L. Multilayered nanocrystalline SnO_2 hollow microspheres synthesized by chemically induced self-assembly in the hydrothermal environment. *J. Phys. Chem. C* **2007**, *111*, 14067−14071.
(31) Yuan, J. J.; Zhang, X. K.; Li, H. D.; Wang, K.; Gao, S. Y.; Yin, Z.; Yu, H. J.; Zhu, X. R.; Xiong, Z. Z.; Xie, Y. M. TiO_2/SnO_2 double-shelled hollow spheres-highly efficient photocatalyst for the degradation of rhodamine B. *Catal. Commun.* **2015**, *60*, 129−133.
(32) Zhang, Y.; Zhou, J. B.; Cai, W. Q.; Zhou, J.; Li, Z. Enhanced photocatalytic performance and degradation pathway of Rhodamine B over hierarchical double-shelled zinc nickel oxide hollow sphere heterojunction. *Appl. Surf. Sci.* **2018**, *430*, 549−560.
(33) Zhou, G. X.; Zhang, Z. L.; Chen, B.; Wang, Y.; Ding, Y.; Zhang, X. L.; Ji, M. Synthesis of double-shelled hollow silica sphere with single-shelled hollow silica sphere and cetyltrimethyl ammonium bromide as dual templates. *Micro. Nano. Letters* **2017**, *12*, 133−135.
(34) He, F. P.; Tian, Y.; Fang, X. B.; Xu, Y. B.; Ye, J. D. Porous calcium phosphate composite bioceramic beads. *Ceram. Int.* **2018**, *44*, 13430−13433.
(35) Nithya, R.; Thirunavukkarasu, A.; Sathya, A. B.; Sivashankar, R. Magnetic materials and magnetic separation of dyes from aqueous solutions: a review. *Environ. Chem. Lett.* **2021**, *19*, 1275−1294.
(36) Thirunavukkarasu, A.; Nithya, R.; Sivashankar, R. A review on the role of nanomaterials in the removal of organic pollutants from wastewater. *Rev. Environ. Sci. Bio.* **2020**, *19*, 751−778.
(37) Cao, M.; Jiang, F.; Wang, C.; Cui, H.; Guo, C.; Chang, Y.; Wang, Z. Preparation, microstructure and mechanical property of double-layered metal-ceramic hollow spheres. *Mater. Sci. Eng., A* **2020**, *780*, 139188.
(38) Azzolina-Jury, F. Novel boehmite transformation into γ-alumina and preparation of efficient nickel base alumina porous extrudates for plasma-assisted CO_2 methanation. *J. Ind. Eng. Chem.* **2019**, *71*, 410−424.
(39) Tregubenko, V. Y.; Udras, I.; Drozdov, V.; Belyi, A. Effect of pseudoboehmite peptization by organic acids on texture characteristics of obtained aluminum oxides. *Russ. J. Appl. Chem.* **2011**, *84*, 9−16.
(40) Dong, Y.; Jiang, H. Y.; Chen, A. N.; Yang, T.; Zou, T. T.; Xu, D. Porous Al_2O_3 ceramics with spontaneously formed pores and enhanced strength prepared by indirect selective laser sintering combined with reaction bonding. *Ceram. Int.* **2020**, *46*, 15159−15166.
(41) Tregubenko, V. Y.; Udras, I.; Belyi, A. Preparation of Mesoporous γ-Al_2O_3 from Aluminum Hydroxide Peptized with Organic Acids. *Russ. J. Appl. Chem.* **2017**, *90*, 1961−1968.
(42) Zhang, H.; Jiang, T.; Yaseen, H. A. S. M.; Zhao, Y.; Wang, S.; Ma, X. Pelletization and attrition of CaO-based adsorbent for CO_2 capture. *Asia-Pac. J. Chem. Eng.* **2021**, *16*, No. e2656.
(43) Sivashankar, R.; Thirunavukkarasu, A.; Nithya, R.; Kanimozhi, J.; Sathya, A. B.; Sivasubramanian, V. Sequestration of methylene blue dye from aqueous solution by magnetic biocomposite: three level Box−Behnken experimental design optimization and kinetic studies. *Sep. Sci. Technol.* **2020**, *55*, 1752−1765.
(44) Van Garderen, N.; Clemens, F. J.; Aneziris, C. G.; Graule, T. Improved γ-alumina support based pseudo-boehmite shaped by micro-extrusion process for oxygen carrier support application. *Ceram. Int.* **2012**, *38*, 5481−5492.
(45) Guo Yin, L.; Jian Ping, Z.; Yu Lin, Z. Pore structure control of activated alumina. *Chin. J. Inorg. Chem.* **2007**, *23*, 563−568.
(46) Tang, G. W.; Zhang, H.; Zhao, Y. H.; Zhang, Y.; Li, X. L.; Yuan, X. Y. Preparation of PLGA scaffolds with graded pores by using a gelatin-microsphere template as porogen. *J. Biomater. Sci. Polym. Ed.* **2012**, *23*, 2241−2257.
(47) Kapur, P.; Fuerstenau, D. Dry strength of pelletized spheres. *J. Am. Ceram. Soc.* **1967**, *50*, 14−18.
(48) Wang, H.; Tian, L.; Huang, Z.; Liang, F.; Guan, K.; Jia, Q.; Zhang, H.; Zhang, S. Molten salt synthesis of carbon-doped boron nitride nanosheets with enhanced adsorption performance. *Nanotechnology* **2020**, *31*, 505606.
(49) Tian, L.; Liang, F.; Dong, L. H.; Li, J. Y.; Jia, Q. L.; Zhang, H. J.; Yan, S.; Zhang, S. W. Preparation and enhanced adsorption properties for CO_2 and dyes of amino-decorated hierarchical porous BCN aerogels. *J. Am. Ceram. Soc.* **2021**, *104*, 1110−1119.
(50) Lei, C. S.; Pi, M.; Xu, D. F.; Jiang, C. J.; Cheng, B. Fabrication of hierarchical porous ZnO-Al_2O_3 microspheres with enhanced adsorption performance. *Appl. Surf. Sci.* **2017**, *426*, 360−368.
(51) Zhang, Y.; Li, X. Preparation of Al_2O_3 hollow microsphere via calcining carbon template and its adsorption application. *Chem. Phys. Lett.* **2019**, *731*, 136589.
(52) Yan, S.; Pan, Y. M.; Wang, L.; Liu, J. J.; Zhang, Z. J.; Huo, W. L.; Yang, J. L.; Huang, Y. Synthesis of low-cost porous ceramic microspheres from waste gangue for dye adsorption. *J. Adv. Ceram.* **2018**, *7*, 30−40.
(53) Fang, J. M.; Huang, X. Y.; Ou Yang, X.; Wang, X. Study of the preparation of γ-Al_2O_3 nano-structured hierarchical hollow microspheres with a simple hydrothermal synthesis using methylene blue as structure directing agent and their adsorption enhancement for the dye. *Chem. Eng. J.* **2015**, *270*, 309−319.
(54) Fan, H. L.; Li, L.; Zhou, S. F.; Liu, Y. Z. Continuous preparation of Fe_3O_4 nanoparticles combined with surface modification by L-cysteine and their application in heavy metal adsorption. *Ceram. Int.* **2016**, *42*, 4228−4237.
(55) Liu, Y.; Luan, J.; Zhang, C.; Ke, X.; Zhang, H. The adsorption behavior of multiple contaminants like heavy metal ions and p-nitrophenol on organic-modified montmorillonite. *Environ. Sci. Pollut. Res. Int.* **2019**, *26*, 10387−10397.
(56) Rajarathinam, N.; Arunachalam, T.; Raja, S.; Selvasembian, R. Fenalan Yellow G adsorption using surface-functionalized green nanoceria: an insight into mechanism and statistical modelling. *Environ. Res.* **2020**, *181*, 108920.
(57) Wu, Y.; Luo, H.; Wang, H. Efficient Removal of Congo Red from Aqueous Solutions by Surfactant-Modified Hydroxo Aluminum/Graphene Composites. *Sep. Sci. Technol.* **2014**, *49*, 2700−2710.
(58) Granados-Correa, F.; Corral-Capulin, N. G.; Olguín, M. T.; Acosta-León, C. E. Comparison of the Cd(II) adsorption processes between boehmite (γ-AlOOH) and goethite (α-FeOOH). *Chem. Eng. J.* **2011**, *171*, 1027−1034.
(59) Nie, L. H.; Tan, Q.; Zhu, W.; Wei, Q.; Lin, Z. K. Fast Adsorption removal of congo red on hierarchically porous γ-Al_2O_3 hollow microspheres prepared by microwave-assisted hydrothermal method. *Acta Phys-Chim. Sin.* **2015**, *31*, 1815−1822.

https://doi.org/10.1021/acsomega.2c04490
ACS Omega 2022, 7, 37629−37639

(60) Ohale, P. E.; Onu, C. E.; Ohale, N. J.; Oba, S. N. Adsorptive kinetics, isotherm and thermodynamic analysis of fishpond effluent coagulation using chitin derived coagulant from waste Brachyura shell. *Chem. Eng. Adv.* **2020**, *4*, 100036.
(61) Li, S.; Zhang, H.; Hu, S.; Liu, J.; Zhu, Q.; Zhang, S. Synthesis of Hierarchical Porous Carbon in Molten Salt and Its Application for Dye Adsorption. *Nanomaterials* **2019**, *9*, 1098.
(62) Zhou, J. B.; Tang, C.; Cheng, B.; Yu, J. G.; Jaroniec, M. Rattle-type carbon−alumina core−shell spheres: synthesis and application for adsorption of organic dyes. *ACS Appl. Mater. Interfaces* **2012**, *4*, 2174−2179.
(63) Ali, I.; Burakova, I.; Galunin, E.; Burakov, A.; Mkrtchyan, E.; Melezhik, A.; Kurnosov, D.; Tkachev, A.; Grachev, V. High-speed and high-capacity removal of methyl orange and malachite green in water using newly developed mesoporous carbon: kinetic and isotherm studies. *ACS Omega* **2019**, *4*, 19293−19306.
(64) Wang, L.; Wang, A. Q. Adsorption properties of Congo Red from aqueous solution onto surfactant-modified montmorillonite. *J. Hazard. Mater.* **2008**, *160*, 173−180.
(65) Zhao, S. Z.; Wen, Y. F.; Du, C. C.; Tang, T.; Kang, D. J. Introduction of vacancy capture mechanism into defective alumina microspheres for enhanced adsorption of organic dyes. *Chem. Eng. J.* **2020**, *402*, 126180.
(66) Pommerenk, P.; Schafran, G. C. Adsorption of inorganic and organic ligands onto hydrous aluminum oxide: evaluation of surface charge and the impacts on particle and NOM removal during water treatment. *Environ. Sci. Technol.* **2005**, *39*, 6429−34.
(67) Young, C.; Zhang, C.; Nisar, A.; Boesl, B.; Agarwal, A. Spark plasma sintered porous aluminum oxide for filtration applications. *Ceram. Int.* **2021**, *47*, 21822−21827.
(68) Cai, W.; Hu, Y.; Chen, J.; Zhang, G.; Xia, T. Synthesis of nanorod-like mesoporous γ-Al_2O_3 with enhanced affinity towards Congo red removal: Effects of anions and structure-directing agents. *CrystEngComm* **2012**, *14*, 972−977.
(69) Meng, F. C.; Rong, G.; Zhang, X. L.; Huang, W. J. Facile hydrothermal synthesis of hierarchically structured γ-AlOOH for fast Congo red removal. *Mater. Lett.* **2014**, *129*, 114−117.
(70) Wang, X.; Zhong, Y. T.; Zhai, T. Y.; Guo, Y. F.; Chen, S. M.; Ma, Y.; Yao, J. N.; Bando, Y.; Golberg, D. Multishelled Co_3O_4-Fe_3O_4 hollow spheres with even magnetic phase distribution: Synthesis, magnetic properties and their application in water treatment. *J.Mater. Chem.* **2011**, *21*, 17680−17687.
(71) Wang, C.; Le, Y.; Cheng, B. Fabrication of porous ZrO_2 hollow sphere and its adsorption performance to Congo red in water. *Ceram. Int.* **2014**, *40*, 10847−10856.
(72) Zhang, J. J.; Yan, X. L.; Hu, M. Q.; Hu, X. Y.; Zhou, M. Adsorption of Congo red from aqueous solution using ZnO-modified SiO_2 nanospheres with rough surfaces. *J. Mol. Liq.* **2018**, *249*, 772−778.
(73) Li, S. S.; Huang, L.; Zhang, H. J.; Huang, Z.; Jia, Q. L.; Zhang, S. W. Adsorption mechanism of methylene blue on oxygen-containing functional groups modified graphitic carbon spheres: Experiment and DFT study. *Appl. Surf. Sci.* **2021**, *540*, 148386.
(74) Li, J. Y.; Tian, L.; Liang, F.; Wang, J. K.; Han, L.; Zhang, J.; Ge, S. T.; Dong, L. H.; Zhang, H. J.; Zhang, S. W. Molten salt synthesis of hierarchical porous N-doped carbon submicrospheres for multifunctional applications: high performance supercapacitor, dye removal and CO_2 capture. *Carbon* **2019**, *141*, 739−747.

https://doi.org/10.1021/acsomega.2c04490
ACS Omega 2022, 7, 37629−37639